Precursor effects, broken local symmetry, and coexistence of order-disorder and displacive dynamics in perovskite ferroelectrics

A. Bussmann-Holder,[1] H. Beige,[2] and G. Völkel[3]
[1]*Max-Planck-Institut für Festkörperforschung, Heisenbergstr. 1, D-70569 Stuttgart, Germany*
[2]*Naturwissenschaftliche Fakultät II, Institut für Physik–Physik Ferroischer Materialien, Martin-Luther-Universität Halle-Wittenberg, Friedemann-Bach-Platz 6, D-06108 Halle/Saale, Germany*
[3]*Fakultät für Physik und Geowissenschaften der Universität Leipzig, Linnéstr. 5, D-04103 Leipzig, Germany*
(Received 11 December 2008; revised manuscript received 27 April 2009; published 20 May 2009)

The dynamical properties of ferroelectric perovskites have typically been classified as being either of order-disorder or displacive type. Here we show that this simple scheme is not generally applicable but that the generic and intrinsic properties of this material class always combine both aspects. Important in this respect is the fact that different length and time scales are associated with the two properties which makes it difficult to observe them with a single experiment. In addition, it is shown that independent of the transition temperature of the respective system precursor dynamics exist which set in approximately 75 K above the actual phase-transition temperature. This theoretical result is supported by measurements of elastic and dielectric coefficients.

DOI: 10.1103/PhysRevB.79.184111 PACS number(s): 77.84.−s, 77.80.Bh, 63.20.Ry

I. INTRODUCTION

Perovskite oxide ferroelectrics are known since almost six decades and belong to one of the most interesting material classes since not only their huge potential of applications is of interest but also their broad range of ground-state properties. Especially, the technological interest in them has increased the research in these compounds in order to overcome problems related to the material optimization. In spite of these enormous theoretical and experimental efforts to understand the properties of ferroelectric perovskites from a microscopic point of view, still a variety of experimental new findings remain unexplained. These are related to the dynamics of the phase transition, namely, whether it is of order-disorder or displacive type.[1] Seemingly controversial experimental data either support a purely displacive mechanism or a transition of the order-disorder type. While long-wavelength testing experiments typically observe perfect mode softening characteristic of the displacive mechanism, local probes support the order-disorder aspect.[1–9] These local probes also suggest that small polarized clusters form far above the transition temperature T_c and grow with decreasing temperature to finally coalesce into a ferroelectric state at T_c.[10] The existence of these pretransitional clusters has already been addressed early on and has been interpreted in terms of a crossover behavior from displacive to order-disorder with special emphasis to the case of $BaTiO_3$.[1,9] More recent data on the same compound are in agreement with these early approaches since, e.g., an anomalous birefringence is present above the transition temperature T_c,[11] which is suggested to be due to the formation of microregions or nanoregions of polar clusters appearing well above T_c. Also the analysis of electron-paramagnetic-resonance (EPR) (Ref. 9) data evidences coexistence regions of different structures within a broad temperature regime which stem from order-disorder dynamics despite of the fact that classical mode softening—indicating the displacive limit—is present.[12,13] In a recent Brillouin-scattering study polar precursors have been detected in the paraelectric phase of $BaTiO_3$ which correlate with the softening of a longitudinal acoustic mode and appear already approximately 80 K above T_c.[14] In an earlier Brillouin-scattering study acoustic-phonon velocities have been measured as a function of pressure.[15] The observed anomaly in one of the eigenmodes has been interpreted as arising from anisotropic fields. Fluctuating polar clusters have also been observed by picosecond x-ray laser speckle technique in the paraelectric phase of $BaTiO_3$ where their size grows upon approaching the instability.[16] Also temperature-dependent measurements of the linear and nonlinear elastic and dielectric coefficients suggest the existence of precursor effects appearing far above the cubic-tetragonal phase transition.[17] These anomalies will be analyzed in detail below. But, not only $BaTiO_3$ exhibits these locally distorted regions well above T_c, there are similar observations for $PbTiO_3$,[18] $PbHfO_3$,[19,20] $CdTiO_3$,[21] superlattices of $SrTiO_3/DyScO_3$,[22] and $SrTiO_3$,[23,24]—all of them showing "classical" mode softening.[25] These data support the conclusion that polar microregions or nanoregions are common to perovskite ferroelectrics and are even generic and intrinsic implying that displacive and order-disorder dynamics do always coexist but may obey different time and length scales.[26,27] This latter conclusion is in contrast to hydrogen bonded ferroelectrics where the same time and length scales have been observed for both dynamics.[28,29]

II. THEORETICAL MODELING

While in previous work the distinction between displacive and relaxor order-disorder-type ferroelectrics has been attributed to the depth of the local double-well potential,[1] it is shown here that precursor dynamics are always present and that these are independent of the shape and the depth of the double-well potential. The appearance of these locally distorted dynamical regions sets in well above the actual instability. This has been shown recently in Ref. 23 to be realized in $SrTi^{16}O_3$ and $SrTi^{18}O_3$. However, this system differs sub-

stantially from typical ferroelectric perovskites since quantum fluctuations suppress the actual instability in the former[30] and dominate the *incomplete* ferroelectric state in the latter. Thus, conclusions reached for $SrTi^{16}O_3$ and $SrTi^{18}O_3$ cannot be generalized for a ferroelectric perovskite oxide which undergoes a real phase transition at temperatures well above the quantum regime. The theoretical modeling is based on the polarizability model[31,32] which has been shown to capture the essential physics of ferroelectrics.[33] The ferroelectric transition temperature is variable in this model through variations in the local double-well potential height. Even though the results, presented below, are obtained on a mean-field level using the self-consistent phonon approximation (SPA), local structural distortions are implicitly obtained through pronounced anomalies in the elastic constants as derived from the dispersion relation of the acoustic mode.[34] The model differs substantially from Φ_4 models typically employed for ferroelectrics since the double-well potential used here is in the relative displacement coordinate between ionic core and its surrounding shell. This shell model representation of ferroelectrics captures essential dynamical charge-transfer effects between the central B transition-metal ion d states and the oxygen ion p states in ABO_3 which crucially influence the dynamical properties.[35] The model Hamiltonian in its pseudo-one-dimensional representation reads[32]

$$H = \frac{1}{2}\sum_n \Big[M_1 \dot{u}_{1n}^2 + m_2 \dot{u}_{2n}^2 + f'(u_{1n+1} - u_{1n})^2 + f(v_{1n} - u_{2n})^2 + f(v_{1n+1} - u_{2n})^2 + g_2 w_{1n}^2 + \frac{1}{2} g_4 w_{1n}^4 \Big], \quad (1)$$

where M_1, m_2 refer to the polarizable cluster mass BO_3 and the A sublattice mass with site n-dependent displacement coordinates $u_{in}, i=1,2$, respectively. The electronic displacement is given by v_{1n}. Nearest-neighbor interactions between the two particles are indirect through the shells and are determined by the harmonic force constant f. Note that this indirect interaction provides important renormalizations of the soft-mode frequency and, in addition, causes a substantial coupling between the acoustic- and the optic-mode frequencies. The next-nearest-neighbor coupling between the polarizable BO_3 units is given by f' and guarantees the stability of the lattice. The double-well potential, which is used here, is in the relative electron-ion displacement coordinate $w_{1n}=v_{1n}-u_{1n}$ and characterized through the attractive harmonic term g_2 and the stabilizing nonlinear fourth-order coupling constant g_4. While interesting superlattice modulations and nonlinear excitations result when exact solutions of the model are tested,[35–37] the use of the SPA admits to calculate the relevant temperature-dependent properties. In the following the SPA is applied since the soft-mode temperature dependence as well as its coupling to the related acoustic mode can be best analyzed. The dispersion relations derived from Hamiltonian (1) are

$$\omega_{1,2}^2 = \frac{1}{2}[\omega_{\mathrm{TO}}^2 + \omega_{\mathrm{TA}}^2] \pm \frac{1}{2}\sqrt{[\omega_{\mathrm{TO}}^2 - \omega_{\mathrm{TA}}^2]^2 + \Delta^2} \quad (2)$$

with $\omega_{\mathrm{TO}}^2 = \frac{1}{m_2}[\frac{4\tilde{f}f}{g}\sin^2 qa + 2\tilde{f}]$, $\omega_{\mathrm{TA}}^2 = \frac{1}{M_1}[4f' \sin^2 qa + 2\tilde{f}]$, $\Delta^2 = \frac{4\tilde{f}^2}{\mu}\cos^2 qa$, and $\tilde{f} = \frac{fg}{(2f+g)}$, where μ is the reduced cell mass and g is defined through $g = g_2 + 3g_4\langle w^2\rangle_T$, which corresponds to a cumulant expansion of the cubic term in w appearing in the equations of motion and has to be calculated self-consistently at each temperature T. The phase-transition temperature T_c is assigned to the condition $g \to 0$, i.e., through the implicit relation

$$0 = g_2 + 3g_4 \sum_{g,j} \frac{\hbar}{2\omega_{q,j}} w_{q,j}^2 \coth\frac{\hbar\omega_{q,j}}{2k_B T_c}, \quad (3)$$

where the sum is over all phonon branches j and momenta q and w is the corresponding eigenvector. By transforming the summation to an integral in q^3 space the approach guarantees that a transition takes place although on the expense of using an isotropic dispersion. Typically, the parameters entering the model are fully determined through experimental data: f is fixed through the optic zone-boundary mode frequency, whereas f' is given by the acoustic zone-boundary mode frequency. g_2, g_4 are determined self-consistently. Since the aim of this paper is to show that local structural instabilities occur far above the long-wavelength-related polar instability, the values of T_c are varied here through the variation in the local double-well potential height.

III. THEORETICAL RESULTS

First the squared soft-mode frequency ω_f^2, which corresponds to the transverse optic mode in the $q=0$ limit of Eq. (2), is calculated as a function of temperature and g_2 and is shown in Fig. 1(a). Since the chosen transition temperatures are not in the quantum limit, mean-field behavior in the temperature dependence is expected, i.e., $\omega_f^2 \approx (T - T_c)$. This is, however, in no case observed over the full temperature regime but deviations appear in the vicinity of T_c and at high temperatures in agreement with experimental observations. These deviations from linearity become more pronounced the lower T_c is and are, as has been shown previously, manifested in the quantum limit where a dimensionality crossover sets in.[23,24,38] At high temperatures the saturation of the soft-mode sets in, which is absent in conventional Φ_4 theories. For all three examples chosen, the Curie constant increases with increasing T_c as shown in Fig. 1(b). The main purpose of calculating the soft-mode frequency as a function of temperature is, however, to show that a long-wavelength instability exists as observed by many experiments. This finding primarily suggests that the transition described here is of the pure displacive type and that this conclusion which is incomplete can be derived from the dispersion of the optic and acoustic modes, which start to couple at finite momentum. As long as the coupling constant g is large as compared to the nearest-neighbor coupling constant, i.e., $T \gg T_c$, this coupling is temperature independent since in this limit Δ is given by $\Delta = (4f^2/\mu)\cos^2 qa$. If the opposite limit applies when T approaches T_c but still being appreciably far away, $\Delta = [(g_2 + 3g_4\langle w^2\rangle_T)^2/\mu]\cos^2 qa$. This provides a temperature- and momentum-dependent coupling which gets pronounced with decreasing temperature and induces momentum-dependent anomalies in the acoustic-mode dispersion. The critical momentum q_c, where these anomalies

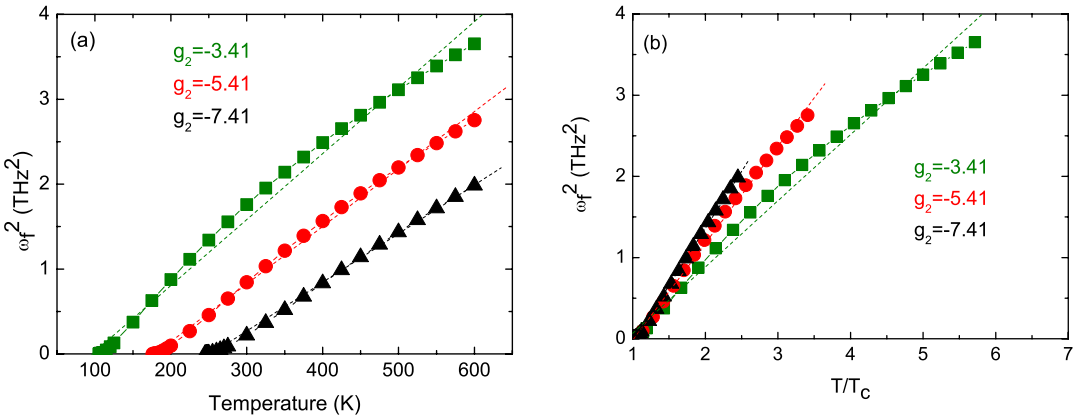

FIG. 1. (Color online) (a) The squared soft-mode frequency ω_f^2 as a function of temperature for three different values of g_2 as indicated in the figure. (b) The same as (a) but with the temperature being normalized to T/T_c.

appear, provides information about the length scales and their local extensions in real space. In order to compare the three cases of different T_c's studied here, the high-temperature limit $T=600$ K is used for the acoustic mode to compare the temperature evolution of the anomaly. This is displayed in Fig. 2 where q_c is shown as a function of normalized temperature. Obviously, for all values of T_c, q_c lies on a universal curve. The farther T is above T_c the larger is the momentum at which the anomaly is present. In addition, q_c converges to a constant value, i.e., $q_c=0.5$ for $T \gg T_c$, which signals the inherent tendency of the system to a doubling of the unit cell corresponding to a zone-boundary instability. Indeed such an instability is observed in many perovskite ferroelectrics and takes place in $SrTiO_3$.[23,30]

Upon decreasing the temperature and approaching T_c, q_c shifts to the long-wavelength limit indicating a coalescence of the local dynamics into a coherently polarized state. The related length scale of these dynamically distorted regions is shown in Fig. 3 which emphasizes the divergent behavior appearing at T_c. It is interesting to note here that a universal behavior is observed in all three cases even though the soft-mode temperature evolution differs substantially from universality. Far above T_c these regions are small and on the order of a few lattice constants only. When the temperature reaches about twice the transition temperature, their spatial dimensions start to grow to be almost doubled at $T/T_c=1.5$. When approaching T_c further their growth is rapid and reaches 10–15 lattice constants at $T/T_c=1.1$ which corresponds in the investigated cases to a temperature window of 10–30 K. A very different response appears when instead of changing the potential height the core-core coupling f' is varied. In that case an extremely complex phase diagram is the consequence.[26] Yet, the common aspect of both approaches is that pretransitional local dynamics occur far above T_c. While the momentum anomaly reveals information about the length scale involved in the local dynamics as quantified above, the frequency value at the anomaly provides information about the time scale: for the long-wavelength soft mode ω_f the time scale is in the THz regime and for the precursor dynamics substantially slower time scales apply which are in the MHz–GHz region. This is shown in Fig. 4 where again these data are compared to the 600 K dispersion of the acoustic mode.

Comparing the temperature dependence of the acoustic-mode frequency at q_c for the three different cases, universality is absent here. For the highest T_c (245 K) the frequency rapidly approaches the value of the harmonic mode whereas this is still substantially smaller in the case of $T_c=105$ K even if the temperature is five times larger than T_c. In spite of these different temperature dependencies a common aspect

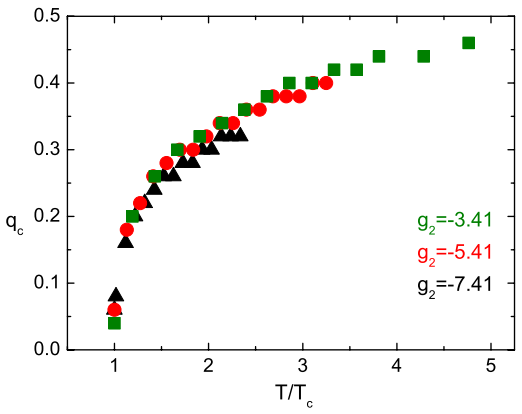

FIG. 2. (Color online) Dependence of the critical momentum q_c on T/T_c for different values of g_2 as indicated in the figure.

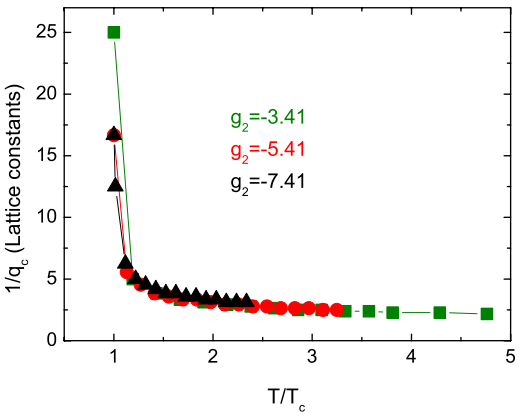

FIG. 3. (Color online) The critical length scale as a function of T/T_c for different values of g_2 as indicated in the figure.

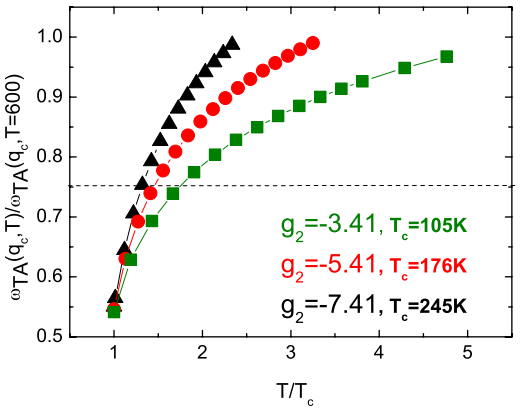

FIG. 4. (Color online) Normalized acoustic-mode frequency $\omega_{\mathrm{TA}}(q_c,T)/\omega_{\mathrm{TA}}(q_c,T=600\ \mathrm{K})$ versus T/T_c for three different values of g_2.

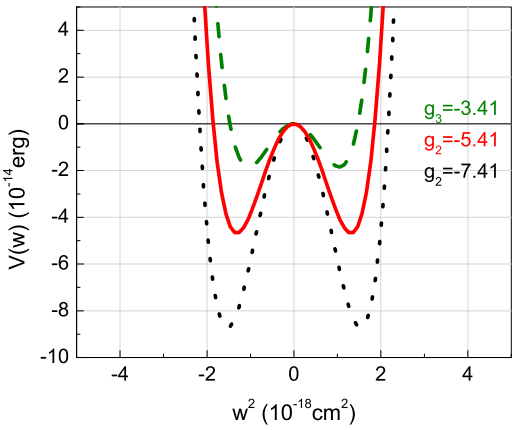

FIG. 5. (Color online) The local double-well potential as a function of the relative coordinate w for three different values of g_2 as indicated in the figure.

of all three cases can be deduced from the result. By defining a minimum softening of 75% as compared to the 600 K mode frequency to be relevant to detect this softening experimentally (which corresponds to a domain size of ~5 lattice constants), the onset temperatures can be derived from Fig. 4. In all cases the precursor dynamics start to develop approximately 75 K prior to the long-wavelength instability. Even if a larger percentage is taken as the relevant one and the temperature scale for the local dynamics increases, a similar trend is observed. This means that the local dynamics develop always almost at the same temperature scale above T_c in the investigated systems.

Another conclusion from the above analysis relates to the role played by the depth of the local double-well potential. While this has been assumed to be decisive for the distinction between relaxational and displacive dynamics,[1] the above results support the viewpoint that independent of the double-well potential depth both dynamics coexist, however, exhibiting different length and time scales, namely, long wavelength for the optic ferroelectric mode and a few lattice constants for the related acoustic mode; THz frequencies for the former and MHz–GHz for the latter. The depths of the double-well potentials used in these calculations differ substantially for the three investigated examples as is shown in Fig. 5.

As has been outlined in Sec. I, experimental data for perovskite ferroelectrics seem to be controversial since long-wavelength testing probes are in support of the displacive nature of the phase transition while local probes corroborate the order-disorder aspect. The above modeling, however, shows that both findings are not controversial but complimentary as the local dynamics coexist with the long-wavelength ones, which evidences that order-disorder and displacive mechanisms are present simultaneously.

IV. THERMODYNAMIC ANALYSIS OF LINEAR AND NONLINEAR DIELECTRIC AND ELASTIC COEFFICIENTS OF $BaTiO_3$

In order to affirm the above-described results, linear and nonlinear elastic and dielectric coefficients have been measured and analyzed for $BaTiO_3$.[17] The analysis of the data is based on the thermodynamic potential function which is expanded in terms of higher orders of the mechanical stress T_j and the electric field strength E_m.[39] The equations of state for the strain S_i and the dielectric displacement D_m are obtained as $S_i=s_{ij}^E T_j+s_{ijk}^E T_j T_k, D_m=\varepsilon_{mn}^T E_n+\varepsilon_{mnp}^T E_n E_p$, where s_{ij}^E, s_{ijk}^E are the second-order linear and third-order nonlinear elastic coefficients, where the latter determines the change in the linear term with mechanical stress T_j. $\varepsilon_{mn}^T, \varepsilon_{mnp}^T$ are the linear and third-order nonlinear dielectric coefficients, respectively. Again, the nonlinear term characterizes the change in the linear dielectric constant with the electric field strength E_m. While the third-order nonlinear elastic coefficients exist for all crystal classes, the nonlinear dielectric coefficient is only observable for crystal classes without a center of symmetry. The temperature dependencies of linear and nonlinear coefficients near first-order phase transitions are obtained from the Landau free-energy thermodynamic potential,

$$G = G_0(T) - \frac{1}{2}s_{ij}^E T_i T_j - \frac{1}{2}\varepsilon_{mn}^T E_m E_n - \frac{1}{3}s_{ijk}^E T_i T_j T_k$$
$$- \frac{1}{3}\varepsilon_{mnp}^T E_m E_n E_p + \frac{1}{2}A_{rr}\eta_r^2 + \frac{1}{4}B_{rrrr}^4\eta_r^4 + \frac{1}{6}C_{rrrrrr}^6\eta_r^6$$
$$- K_{ri}T_i\eta_r - \alpha_{rmn}E_m\eta_r - M_{rij}T_i T_j\eta_r - \beta_{rmn}E_m E_n\eta_r$$

TABLE I. Temperature dependence of the elastic and dielectric coefficients for a noncentrosymmetric system: the first row denotes the respective coefficient, while the second row denotes the corresponding theoretically derived T dependence.

Coefficient	T dependence
$\tilde{s}_{ii}^E - s_{ii}^E$	$\frac{K_{ri}^2}{\alpha_{rr}(T-T_0)}$
$\tilde{\varepsilon}_{mm}^T - \varepsilon_{mm}^T$	$\frac{\alpha_{rm}^2}{\alpha_{rr}(T-T_0)}$
$\tilde{s}_{iii}^E - s_{iii}^E$	$\frac{3K_{ri}M_{rii}}{\alpha_{rr}(T-T_0)} + \frac{3K_{ri}^2 N_{rri}}{[\alpha_{rr}(T-T_0)]^2}$

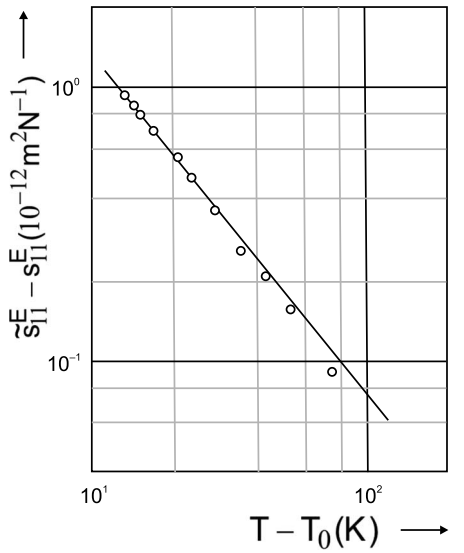

FIG. 6. Double-logarithmic plot of the linear elastic coefficient versus $(T-T_0)$.

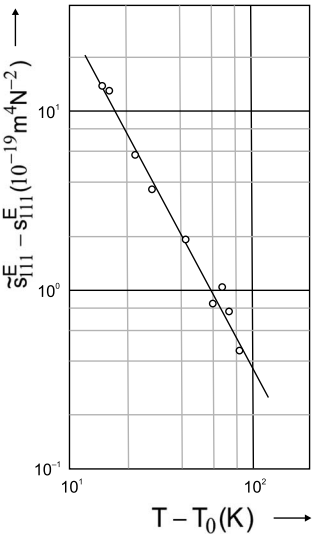

FIG. 7. Double-logarithmic plot of the nonlinear elastic coefficient versus $(T-T_0)$.

$$- N_{rri}T_i\eta_r^2 - \gamma_{rrm}E_m\eta_r^2 - 2V_{rim}T_iE_m\eta_r + \cdots . \tag{4}$$

Here η_r is the order parameter and the coefficients $K_{ri}, \alpha_{rm}, M_{rij}, \beta_{rmn}, N_{rri}, \gamma_{rrm}, V_{rmi}$ couple the order parameter with the electric field strength and the mechanical stress. All coefficients with the exception of A_{rr} are temperature independent[40] and $A_{rr}=A_{rr}(T-T_0)$. The T dependencies of the nonlinear elastic and dielectric coefficients are derived from the following relations:

$$\tilde{s}^E_{ij} = \frac{\partial S_i}{\partial T_j} + \frac{\partial S_i}{\partial \eta_r}\frac{\partial \eta_r}{\partial T_j}, \quad \tilde{\varepsilon}^T_{mn} = \frac{\partial D_m}{\partial E_n} + \frac{\partial D_m}{\partial \eta_r}\frac{\partial \eta_r}{\partial E_n}, \quad \tilde{s}^E_{ijk} = \frac{1}{2}\left[\frac{\partial \tilde{s}^E_{ij}}{\partial T_k} + \frac{\partial \tilde{s}^E_{ij}}{\partial \eta_r}\frac{\partial \eta_r}{\partial T_k}\right], \quad \tilde{\varepsilon}^T_{mnp} = \frac{1}{2}\left[\frac{\partial \tilde{\varepsilon}^T_{mn}}{\partial E_p} + \frac{\partial \tilde{\varepsilon}^T_{mn}}{\partial \eta_r}\frac{\partial \eta_r}{\partial E_p}\right] \tag{5}$$

and are summarized in Table I for the paraelectric phase.

Since $BaTiO_3$ is centrosymmetric in the paraelectric phase, the coupling coefficients $K_{ri}, M_{rij}, \beta_{rmn}, \gamma_{rmm}$ are zero. The resulting temperature dependencies are listed in Table II

TABLE II. Temperature dependence of the elastic and dielectric coefficients in the cubic phase: the first row denotes the coefficient, the second row provides its theoretical T dependence, and the third row corresponds to the experimentally observed one.

T dependence		
Coefficient	Theory	Experiment
$\tilde{s}^E_{ii}-s^E_{ii}$	0	$\approx(T-T_0)^{-1}$
$\tilde{\varepsilon}^T_{mm}-\varepsilon^T_{mm}$	$\frac{\alpha^2_{rm}}{\alpha_{rr}(T-T_0)}$	$\approx(T-T_0)^{-1}$
$\tilde{s}^E_{iii}-s^E_{iii}$	0	$\approx(T-T_0)^{-2}$

and contrasted there to the experimentally observed T dependencies which are also displayed in Figs. 6–8.

Opposite to the theoretically derived results, the experimentally determined coefficients are finite above T_c and exhibit a substantial T dependence (Figs. 6–8). This anomalous behavior is analogous for the elastic and nonlinear dielectric coefficients.[17] The reason for these finite coupling coefficients must be local symmetry breaking caused by precursor formation as predicted theoretically. As seen in Figs. 6–8 the onset temperature for precursor effects starts approximately 80 K above the actual structural instability. This temperature range is in full agreement with the above-derived theoretical temperature regime. In addition similar findings have been seen in Ref. 14.

V. CONCLUSIONS

In conclusion, it has been shown that within the framework of the polarizability model soft-mode behavior, the characteristic of displacive dynamics can well coexist with

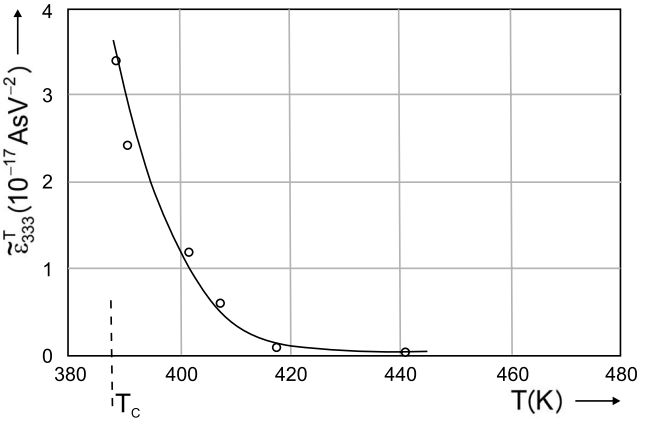

FIG. 8. Nonlinear dielectric coefficient as a function of the temperature for $T>T_c$.

order-disorder dynamics over a substantial temperature range. Experimental support for local symmetry breaking has been given through measurements and the analysis of the elastic and nonlinear dielectric coefficients (Figs. 6–8) which according to symmetry considerations should vanish in the cubic phase but are finite in experiments.[17] While early on ferroelectric phase transitions have been classified in terms of either order-disorder or displacive, it has been shown here that both types of dynamics exist in parallel. However, since both dynamics occur on different time and length scales (THz versus MHz–GHz and long wavelength versus a few lattice constants), a single experiment testing a limited length or time window will see only one component. As such it is difficult to infer from such an experiment on the nature of the phase transition. Further, it is concluded that local dynamical precursor domains are common to perovskite ferroelectrics. These domains grow upon approaching T_c to coalesce into a homogeneously polarized state at T_c. Seemingly, a certain analogy to relaxor ferroelectrics exists to the above modeling since polar nanoregions develop well above T_c in relaxors and cause the frequency dispersion of the dielectric constant. An important distinction to relaxors is, however, that in relaxors the distorted regions develop around a dopant are almost static and have spatially varying dimensions. In the above approach these distorted regions are dynamical, thus not giving rise to a frequency-dependent dielectric response, and have almost identical spatial spread. Also, they are not a consequence of doping but arise intrinsically through optic-acoustic mode-mode coupling.[41]

ACKNOWLEDGMENT

It is a pleasure to acknowledge stimulating discussions with K. A. Müller.

[1] K. A. Müller and W. Berlinger, Phys. Rev. B **34**, 6130 (1986).
[2] K. A. Müller, W. Berlinger, K. W. Blazey, and J. Albers, Solid State Commun. **61**, 21 (1987).
[3] K. A. Müller and J. C. Fayet, in *Structural Phase Transitions II*, edited by K. A. Müller and H. Thomas (Springer Verlag, Berlin, 1991), pp. 1–82.
[4] R. Comes, M. Lambert, and A. Guinier, Solid State Commun. **6**, 715 (1968).
[5] B. Ravel, E. A. Stern, R. I. Verdinskii, and V. Kraizman, Ferroelectrics **206**, 407 (1998).
[6] B. Zalar, V. V. Laguta, and R. Blinc, Phys. Rev. Lett. **90**, 037601 (2003).
[7] B. Zalar, A. Lebar, J. Seliger, R. Blinc, V. V. Laguta, and M. Itoh, Phys. Rev. B **71**, 064107 (2005).
[8] A. S. Chaves, F. C. S. Barreto, R. A. Nogueira, and B. Zeks, Phys. Rev. B **13**, 207 (1976).
[9] G. Völkel and K. A. Müller, Phys. Rev. B **76**, 094105 (2007).
[10] G. Geneste and J. M. Kiat, Phys. Rev. B **77**, 174101 (2008).
[11] A. Ziębińska, D. Rytz, K. Szot, M. Górny, and K. Rolder, J. Phys.: Condens. Matter **20**, 142202 (2008).
[12] W. Cochran, Adv. Phys. **9**, 387 (1960).
[13] J. Harada, J. D. Axe, and G. Shirane, Phys. Rev. B **4**, 155 (1971).
[14] J.-H. Ko, S. Kojima, T.-Y. Koo, J. H. Jung, C. J. Won, and N. J. Hur, Appl. Phys. Lett. **93**, 102905 (2008).
[15] T. Ishidate and S. Sasaki, Phys. Rev. Lett. **62**, 67 (1989).
[16] R. Z. Tai, K. Namikawa, A. Sawada, M. Kishimoto, M. Tanaka, P. Lu, K. Nagashima, H. Maruyama, and M. Ando, Phys. Rev. Lett. **93**, 087601 (2004).
[17] H. Beige and G. Schmidt, Ferroelectrics **41**, 39 (1982).
[18] J. Kwapuliński, M. Pawełczyk, and J. Dec, Ferroelectrics **192**, 307 (1997).
[19] J. Kwapuliński, J. Kusz, H. Böhm, and J. Dec, J. Phys.: Condens. Matter **17**, 1825 (2005).
[20] J. Kwapuliński, M. Pawelczyk, and J. Dec, J. Phys.: Condens. Matter **6**, 4655 (1994).
[21] V. I. Torgashev, Y. I. Yuzyuk, V. B. Shirokov, V. V. Lemanov, and I. E. Spektor, Phys. Solid State **47**, 337 (2005).
[22] P. Kužel, C. Kadlec, F. Kadlec, J. Schubert, and G. Panaitov, Appl. Phys. Lett. **93**, 052910 (2008).
[23] A. Bussmann-Holder, H. Büttner, and A. R. Bishop, Phys. Rev. Lett. **99**, 167603 (2007).
[24] A. Bussmann-Holder and A. R. Bishop, Europhys. Lett. **76**, 945 (2006).
[25] A. Bussmann-Holder, H. Büttner, and A. R. Bishop, J. Phys.: Condens. Matter **12**, L115 (2000).
[26] A. Bussmann-Holder and A. R. Bishop, Ferroelectrics **378**, 42 (2009).
[27] M. Stachiotti, A. Dobry, R. Migoni, and A. Bussmann-Holder, Phys. Rev. B **47**, 2473 (1993).
[28] N. Dalal, A. Klymachyov, and A. Bussmann-Holder, Phys. Rev. Lett. **81**, 5924 (1998).
[29] A. Bussmann-Holder and K. H. Michel, Phys. Rev. Lett. **80**, 2173 (1998).
[30] K. A. Müller and H. Burkard, Phys. Rev. B **19**, 3593 (1979).
[31] R. Migoni, H. Bilz, and D. Bäuerle, Phys. Rev. Lett. **37**, 1155 (1976).
[32] H. Bilz, G. Benedek, and A. Bussmann-Holder, Phys. Rev. B **35**, 4840 (1987).
[33] A. Bussmann-Holder and H. Büttner, Nature (London) **360**, 541 (1992).
[34] A. Bussmann-Holder, Phys. Rev. B **56**, 10762 (1997).
[35] A. Bussmann-Holder and A. R. Bishop, Phys. Rev. B **56**, 5297 (1997).
[36] G. Benedek, A. Bussmann-Holder, and H. Bilz, Phys. Rev. B **36**, 630 (1987).
[37] A. Bussmann-Holder, A. R. Bishop, and G. Benedek, Phys. Rev. B **53**, 11521 (1996).
[38] A. Bussmann-Holder and A. R. Bishop, Phys. Rev. B **78**, 104117 (2008).
[39] V. E. Ljamov, J. Acoust. Soc. Am. **52**, 199 (1972).
[40] Yu. I. Sirotin and L. Shaskol'skaya, *Principles of Crystal Physics* (Nauka, Moscow, 1975) (in Russian).
[41] A. Bussmann-Holder and A. R. Bishop, Phys. Rev. B **70**, 184303 (2004).